First-principles investigations of the electronic structure and magnetocrystalline anisotropy in strained magnetite Fe_3O_4

Horng-Tay Jeng*
Physics Division, National Center for Theoretical Sciences, Hsinchu, Taiwan 30043, Republic of China

G. Y. Guo†
Department of Physics, National Taiwan University, Taipei, Taiwan 10617, Republic of China

(Received 9 October 2000; revised manuscript received 21 September 2001; published 19 February 2002)

The electronic structure and magnetocrystalline anisotropy energy of strained fcc Fe_3O_4 have been studied by using the linear muffin-tin orbital method within density functional theory. A uniaxial strain applied along the [001] direction of the magnetite is considered. It is found that the applied strain would initially reduce the calculated band gap of the majority spin and then turn the half-metallic behavior in the cubic limit into the normal metallic state at high in-plane strains of -1.3% and 2.1%. The calculated fourth-order anisotropy constant K_1 of cubic Fe_3O_4 is in fair agreement with the experimental value. The magnitude of K_1 appears to be suppressed under large extensive lateral strains. The second order uniaxial anisotropy constant K_{out} is positive for extensive in-plane strains and is negative for compressive in-plane strains. The positive value of K_{out} minus the shape anisotropy indicates that an Fe_3O_4 film under an extensive in-plane strain larger than 0.2% would show the perpendicular magnetization, in good agreement with recent experiments on Fe_3O_4 films on MgO(100) and CoO(100). Interestingly, site decomposition shows that the *A*- and *B*-site Fe atoms in the strained magnetite have comparable anisotropy energies but with the opposite signs, while the oxygen's contribution is negligible. This implies that under an extensive lateral strain, the *B*-site irons would favor perpendicular magnetization while the *A*-site irons would prefer an in-plane magnetization. The total K_{out} is dictated by that of the *B*-site irons due to their number being twice that of the *A*-site irons.

DOI: 10.1103/PhysRevB.65.094429 PACS number(s): 75.50.−y, 71.20.−b, 75.30.Gw

I. INTRODUCTION

Magnetite (Fe_3O_4) is the earliest discovered magnet (~1500 B.C.). It crystallizes in the inverse cubic spinel structure ($Fd3m$) above the so-called Verwey transition temperature (120 K). As shown in Fig. 1, the oxygen atoms form in the close-packed face-centered-cubic (fcc) lattices with the iron atoms occupying the interstitial positions.[1] Each cubic spinel cell contains eight interpenetrating oxygen fcc cells. The tetrahedral *A* sites, occupied by one-third of the iron atoms, form a diamond structure. The remaining Fe atoms are located at the octahedral *B* sites with the nearest-neighbor atoms lined up as strings along six different [110] directions. The ferromagnetic moments on the *A* and *B* sites align antiparallel to each other, thereby forming a ferrimagnet with a saturation magnetic moment of $\sim 4\mu_B$ (Bohr magneton) per formula unit (fu).[2,3] There are a few known half-metallic materials which combine full spin polarization with high Curie temperatures (>300 K) such as the manganese perovskites, the spinel Fe_3O_4, CrO_2, and several Heusler compounds (e.g., PtMnSb). As a half-metallic material, Fe_3O_4 shows normal metallic behavior in the minority spin, while at the same time there is a gap of ~0.5 eV in the majority spin at the Fermi level. From an itinerant point of view, the high conductivity (~250 $\Omega^{-1}\,\mathrm{cm}^{-1}$) (Ref. 2) of the high-temperature phase is a natural consequence of the partially filled $3d$ band of the *B*-site Fe atoms.[4,5] The Verwey transition to the low-temperature phase, which is characterized by a metal-insulator transition accompanied with a structural change from cubic to monoclinic,[1,6,7] is presumably a consequence of a band splitting caused by electron correlations and/or electron-phonon interactions.[8] Whereas in the ionic model the high-temperature conductivity is assumed to come from the electron hopping between the Fe^{3+} and Fe^{2+} ions in the octahedral *B*-site strings, while the Verwey transition is interpreted as an order-disorder transformation on the *B*-site Fe ions.[1] Though extensive studies of magnetite with considerable effort have been carried out over the past 50 years

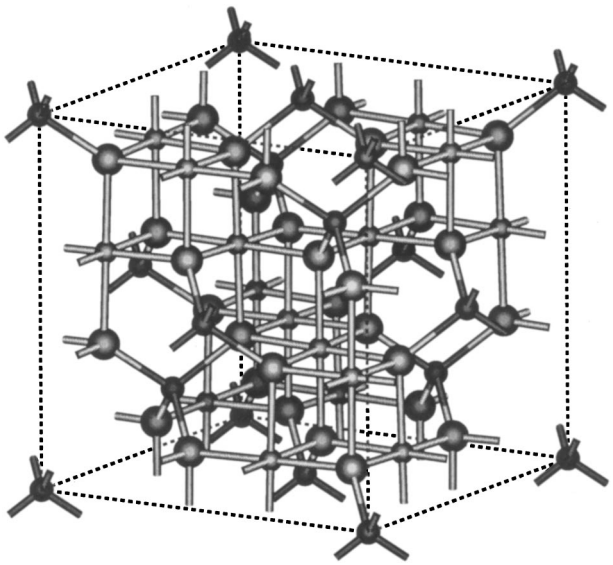

FIG. 1. Crystal structure of Fe_3O_4. Big balls denote oxygen atoms, small dark balls denote *A*-site (tetrahedral) iron atoms, and small light balls denote *B*-site (octahedral) iron atoms.

(see, e.g., Refs. 9–11 and references therein), the Verwey transition remains a challenging problem to be solved. Because of the interesting electronic, magnetic, and transport properties as well as the potential industrial applications in magnetic multilayer devices, magnetite has still attracted much attention in recent years.[12–24]

The continuous improvement of deposition techniques in the last decade has made it possible to prepare artificial layered structures including not only metallic but also oxide magnetic thin films and multilayers. By growing in the form of thin films, the interesting magnetic and electronic properties of magnetite could possibly be manipulated. For ensuring a good epitaxy, ultrathin magnetic structures are commonly composed of magnetic and nonmagnetic layers that are chosen for their compatible lattice parameters. Fe_3O_4 thin films have been prepared on MgO single-crystal substrates, which are ideal templates for cubic oxide spinels because of the close lattice matches, by molecular-beam epitaxy (MBE) or other deposition techniques.[13,14,18,22,23] Several other substrates for growing Fe_3O_4 thin films, such as NiO,[12,15] CoO,[19] Pt,[17,20,21] and Mn_3O_4,[24] have also been reported. However, lattice mismatches of even a few percent in growing thin films on various substrates are unavoidable. The lattice mismatch strains could induce significant effects on the magnetocrystalline anisotropy, on the easy direction of magnetization, and even on the band structure.

The band structure of the high-temperature conducting phase of magnetite has been calculated self-consistently within the framework of the local-spin-density approximation (LSDA) by the augmented plane-wave (APW) method,[4] the augmented spherical-wave (ASW) method,[5,25] and also the linear muffin-tin orbital (LMTO) method.[26] These calculations all give a consistent half-metallic result for the cubic phase. Although there are basic differences between the itinerant electron and localized ionic models, band structure calculations give a magnetic moment of $4\mu_B$/f.u., which is exactly the same as given by the ionic model. On the other hand, experiments such as photoemissions,[17,27,28] spin-polarized photoelectron spectra,[29] and neutron diffraction[30] and also recent neutron diffuse scattering[16] and resonant x-ray scattering[31] all suggest that the itinerant electron model is perhaps more adequate than the localized electron model.

The magnetocrystalline anisotropy energy, which arises mainly from the spin-orbit coupling correction to the Hamiltonian, is a very small correction to the magnetic energy. There have been many measurements on magnetic anisotropy constants for both the high- and low-temperature phases of magnetite.[32–34] Recent experiments on the anisotropy of magnetite are focused on, for example, transport, nonstoichiometric, or doping effects.[3,11,18,35–37] Because of the large amount of computing requirements, reliable anisotropy calculations are possible only in recent years.[38–41] Although the magnetic anisotropy has been investigated experimentally for a long time, there is, to our knowledge, no available theoretical result for magnetite yet. This is certainly related to the difficulties of dealing with the large lattice cell of the spinel structures as well as of calculating the very small energy differences between different magnetization orientations with a sufficient accuracy. It is the purpose of this work to investigate the influences of the lattice mismatch strains on the electronic structure and on the magnetocrystalline anisotropy energy of Fe_3O_4 from first principles.

The rest of this paper is organized as follows. In the next section, we briefly summarize the magnetocrystalline anisotropy theory, the band structure method used, and computational details. The calculated electronic structure and magnetic anisotropy energies of both the cubic phase and strained structures are presented and discussed in detail in Sec. III. The conclusions are given in Sec. IV.

II. THEORY AND COMPUTATIONAL DETAILS

Let us consider a magnetite thin film in high-temperature fcc phase on a given substrate with a close lattice match within a few percent. Lattice strains are subsequently induced in the magnetite thin film by the lattice mismatch at the interface. In this paper, we focus on the effects of these lattice mismatch strains on the electronic and magnetism in the magnetite thin film only. Thus we neglect the effects of surface and interface though they can affect the electronic structure and also contribute to the magnetic anisotropy. This is equivalent to considering a strained infinite Fe_3O_4 crystal. It is expected that the results of the present theoretical calculations could be applied to thick magnetite films of a few nanometers and would help to better understand the important effects of the strains in the magnetite films of all thickness since there is no previous theoretical work yet. Under an applied uniaxial strain along the [001] (normal) direction of Fe_3O_4 thin film, the fcc lattice is reduced to the body-centered-tetragonal (bct) lattice of a lower symmetry. By varying the c/a ratio with the volume of unit cell unchanged, the corresponding in-plane (lateral) strain $(\varepsilon=[\sqrt{2}/(c/a)]^{1/3}-1)$ of desired percentage can thus be produced.

For a cubic crystal bearing a uniaxial strain along the [001] direction, the perturbed energy is given by (e.g., Ref. 41)

$$\Delta E = K_1(\beta_x^2\beta_y^2+\beta_y^2\beta_z^2+\beta_z^2\beta_x^2)-K_{\text{out}}\beta_z^2, \tag{1}$$

where $\beta_x, \beta_y, \beta_z$ are the direction cosines of the magnetization relative to the crystalline axes, and K_{out} and K_1 are, respectively, the second- and fourth-order anisotropy constants in the spin-orbit coupling. Consider the three directions [100], [001], and [110] of magnetization. The corresponding total energies are, respectively,

$$E_{[100]}=E_0, \tag{2}$$

$$E_{[001]}=E_0-K_{\text{out}}, \tag{3}$$

$$E_{[110]}=E_0+\frac{K_1}{4}, \tag{4}$$

where E_0 is the unperturbed energy. Therefore the anisotropy constants can be expressed by

$$K_{\text{out}}=E_{[100]}-E_{[001]}, \tag{5}$$

$$K_1=4(E_{[110]}-E_{[100]}). \tag{6}$$

We first performed all-electron self-consistent electronic structure calculations for each considered strain by using the well-established LMTO method.[42] These *ab initio* calculations are based on local-spin-density functional theory with Vosko-Wilk-Nusair (VWN) parametrization of local density exchange-correlation energy potential.[43] All the scalar-relativistic terms—namely, Darwin and mass-velocity corrections—were included in these calculations. In the cubic structure, the positions of the *A*-site Fe atoms in the magnetite are $\pm(1/8,1/8,1/8)a$, while for *B*-site Fe atoms, they are $(0,0,1/2)a$, $(1/4,0,3/4)a$, $(0,1/4,3/4)a$, and $(1/4,3/4,0)a$. The oxygen atoms are located at $\pm(u+1/4,u+1/4,u+1/4)a$, $\pm(u+1/4,-u,-u)a$, $\pm(-u,u+1/4,-u)a$, and $\pm(-u,-u,u+1/4)a$. Here the experimental lattice constant $a=8.39$ Å $=15.86a_0$ (Bohr radius) and parameter $u=0.0048$ were used.[44] The atomic sphere radius of $2.662a_0$ from the bulk Fe was used for both the *A*- and *B*-site Fe atoms. The remaining space of the unit cell is occupied by the oxygen spheres with a radius of $2.5a_0$. The basis functions used in the calculations were the *s*, *p*, and *d* muffin-tin orbitals. The analytic tetrahedron method was used to perform the Brillouin-zone (BZ) integrations.[45] The number of *k* points over the irreducible wedge (IW) used in the self-consistent calculations was about 600 over 1/16 of the body-centered-tetragonal BZ. The total energy convergence is within 10^{-5} eV/f.u. both with respect to the self-consistent iterations and to the number of *k* points used.

Because of the shear size of the unit cell of the magnetite and the smallness of the magnetic anisotropy energy, it is extremely time consuming to obtain an accurate self-consistent total energy for each magnetization direction. Therefore, as in many previous calculations,[38,40,41,46,47] we used the so-called force theorem[38] to calculate the magnetocrystalline anisotropy energy, as described below. After the self-consistent calculation for each strain considered, we used the resultant self-consistent potential and performed the fully relativistic (i.e., including the spin-orbit coupling) band structure calculation once for each of the [100], [001], and [110] magnetization orientations. The treatment of the spin-orbit coupling has already been described by Andersen.[42] The magnetocrystalline anisotropy was obtained as the difference in the eigenvalue sums between the two magnetization directions considered. There have been several investigations[46,48,49] examining theoretically and numerically the validity of the force theorem. It was found that the force theorem is a good approximation to the fully self-consistent total-energy calculation of the anisotropy energy in second order in the spin-orbit coupling (i.e., the anisotropy energy in a system with a symmetry lower than the cubic one). Earlier numerical calculations[48] also showed that the force theorem is a good approximation to the anisotropy energy in fourth order in the spin-orbit coupling (i.e., the cubic fourth-order anisotropy constant), though recent analytical calculations[49] indicated that the cubic fourth-order anisotropy constant might not be reliably given by the force theorem. As a result, the force theorem has been used in many magnetocrystalline anisotropy energy calculations[38,40,41,46,47] because of much less computational effort needed. For the magnetocrystalline anisotropy energy calculations, the number of *k* points over the IW used was approximately 1200 over 2/16 BZ for the [100], [110], and [001] orientations. The calculated out-of-plane anisotropy constant K_{out} is well converged (within 10^{-4} eV/f.u.) with respect to the number of *k* points used. Because of the numerical difficulties of achieving an accuracy well within 10^{-5} eV in the anisotropy energy calculations, the calculated K_1 in high extensive in-plane strain regime ($>2.8\%$) somehow oscillates considerably with the number of *k* points used. Nonetheless, the calculated K_1 in the other regions converged to within 20%. Furthermore, the overall trend of the cubic anisotropy constant K_1 as a function of strain reported below should be reliable.

III. RESULTS AND DISCUSSION

A. Electronic structure of the cubic phase

Let us first summarize the results for the high-temperature cubic phase (unstrained) of magnetite before discussing the effects of the lattice mismatch strains. The self-consistent (scalar-relativistic) band structure and density of states (DOS) of the cubic fcc Fe_3O_4 are shown in Figs. 2 and 3, respectively. For comparisons with the strained bct Fe_3O_4 of a lower symmetry, the band structure of the cubic Fe_3O_4 along the symmetry lines in the bct Brillouin zone are also shown in the lower panels of Fig. 2. As can be seen in the figures, the present results are consistent with previous *ab initio* calculations,[4,5,25,26] though the computational methods used are quite different. The most pronounced feature of the electronic structure is that magnetite would be a half-metallic material with conductivity resulting only from the partially filled minority-spin Fe(B) $3d$ band. This band is dominated by three off-axial $3d$-t_{2g} orbitals (Fig. 2), which is consistent with the geometry of the spinel structure depicted in Fig. 1 that the conducting *B*-site strings are along the six off-axial [110] directions. For the majority spin, the Fe(B) $3d$-e_g band, which is characterized by insignificant overlaps between axial e_g orbitals of the nearest Fe(B) neighbors, is 0.14 eV below the Fermi level with relatively narrow bandwidth. This results in an insulating majority spin with a band gap of 0.54 eV at the Fermi level, being in the same order of magnitude as that of many semiconductors. As shown in Fig. 3, DOS for the majority and minority spins are asymmetric near the Fermi level, resulting from the antiparallel magnetic coupling between *A*- and *B*-site Fe atoms.

The spin magnetic moments of the cubic magnetite calculated scalar relativistically in the present and previous calculations are listed in Table I. Since the magnitudes of the calculated magnetic moments depend slightly on the choice of the muffin-tin sphere radii, they are different in the different calculations. Nonetheless, for the *A*-site Fe atoms, the spin moment ranging from $3.4\mu_B$ to $3.7\mu_B$ from different band calculations is in rather good agreement with the experimental moment of $3.8\mu_B$.[30] Note that the value from the localized ionic model would be $5\mu_B$. Because of the half-metallic character of the scalar-relativistic band structure, the total magnetic moment is, as it should be, an integer of $4\mu_B$/f.u. Table I also lists the spin and orbital magnetic moments calculated fully relativistically for the [001] magnetization. Clearly, the effect of the spin-orbit coupling is small

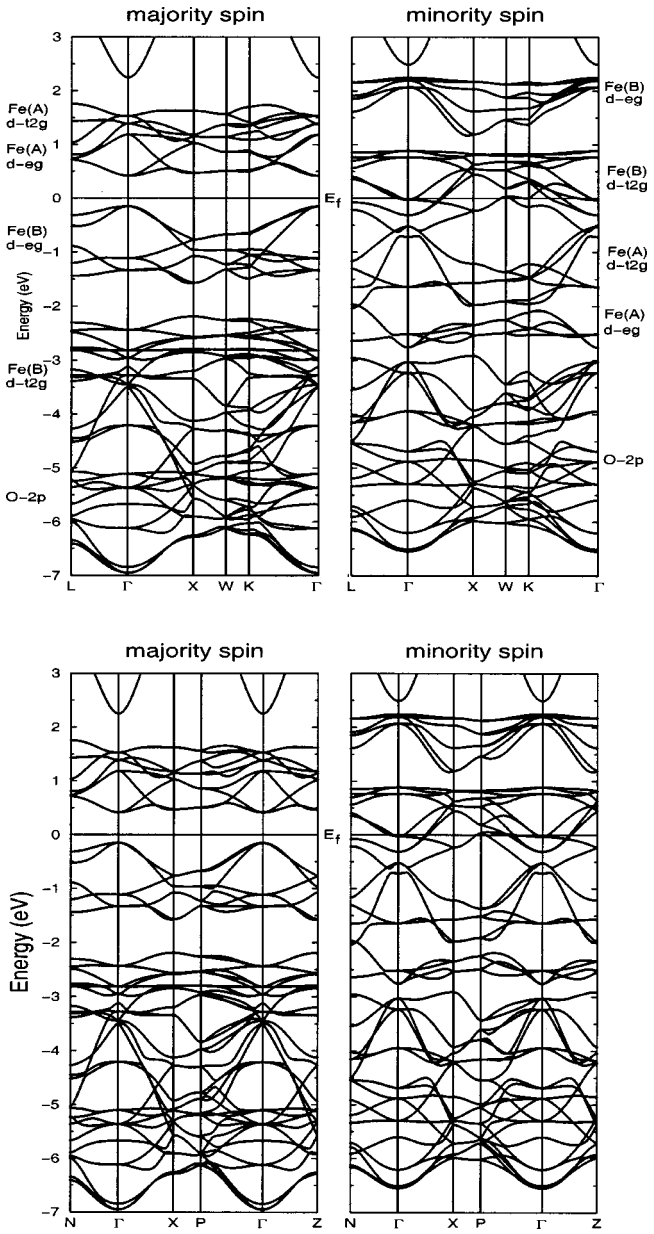

FIG. 2. Band structure of cubic Fe_3O_4 along the fcc symmetry lines (upper panels) and along the bct symmetry lines (lower panels). The Fermi level is at zero energy.

and hence affects the spin magnetic moments only slightly. The calculated orbital magnetic moments on both the *A*- and *B*-site Fe atoms are smaller than that of bulk iron.[48] The fully relativistic band structure is nearly identical to that obtained by superposing the majority-and minority-spin band structures (Fig. 2) and hence is not shown. Note that no fully relativistic spin-polarized band structure calculation for magnetite has been reported. We are not aware of any measurement of the orbital magnetic moments in the magnetite either.

B. Electronic structure under strain

We considered both the positive (extensive) and the negative (compressive) lateral strains in the (001) plane of Fe_3O_4 with the cell volume unchanged, in view of magnetite (001) films grown on various substrates such as Mn_3O_4, NiO, MgO, and CoO with lattice mismatches of −3.2%, −0.69%, 0.36%, and 1.6%, respectively. For simplicity, strain will al-

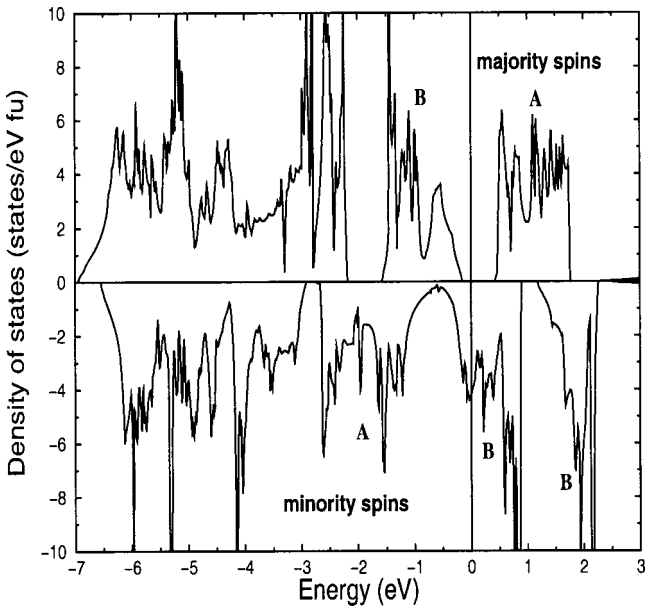

FIG. 3. Spin-decomposed densities of states for unstrained cubic Fe_3O_4. *A* and *B* indicate Fe(*A*) and Fe(*B*) 3*d* dominant bands, respectively. The Fermi level is at zero energy.

TABLE I. Total and site-decomposed spin magnetic moments (M_s) in cubic Fe_3O_4 from the present and previous calculations. Also listed are total and site-decomposed spin (M_s^r) and orbital (M_o^r) magnetic moments for [001] magnetization calculated fully relativistically from the present work.

Atom	M_s^r (μ_B)	M_o^r (μ_B)	M_s (μ_B)	
Fe(*A*)			−3.67[a]	(×1)
			−3.46[b]	
			−3.37[c]	
	−3.40	−0.021	−3.41[d]	
Fe(*B*)			3.67[a]	(×2)
			3.57[b]	
			3.63[c]	
	3.49	0.037	3.49[d]	
O			0.09[a]	(×4)
			0.10[b]	
			0.01[c]	
	0.10	0.000	0.11[d]	
Outer region			−0.03[a]	
			−0.09[b]	
			0.07[c]	
Total	3.99	0.05	4.00	/Fe_3O_4

[a]Reference 4.
[b]Reference 26.
[c]Reference 5.
[d]This work.

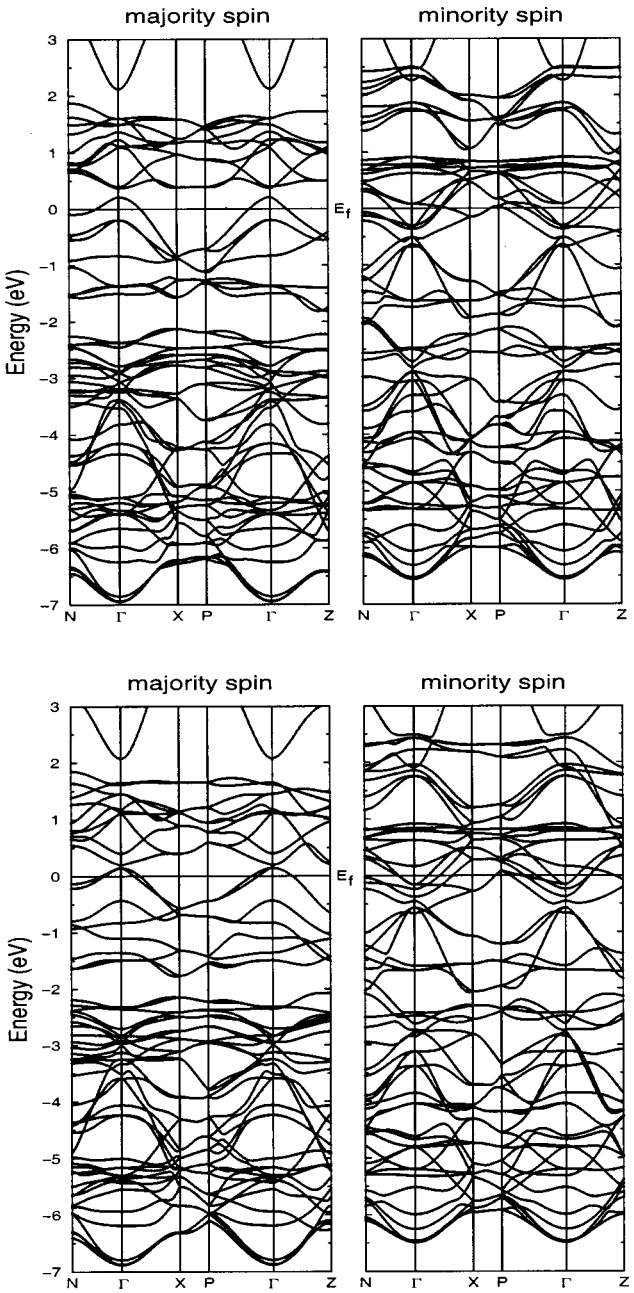

FIG. 4. Band structure of Fe_3O_4 under lateral strains of -3.1% (upper panels) and of 3.6% (lower panels). The Fermi level is at zero energy.

ways be referred to the elastic lateral strain in the rest of this paper unless stated otherwise.

To illustrate the effects of the strains on the electronic structure, the energy bands of Fe_3O_4 under lateral strains of -3.1% and of 3.6% along the symmetry lines in the bct Brillouin zone are plotted in the upper and lower panels of Fig. 4, respectively. As compared with the cubic energy bands along the bct symmetry lines plotted in the lower panels of Fig. 2, the most visible change is in the majority-spin Fe(B) $3d$-e_g band near the Fermi level and the minority-spin Fe(B) $3d$-e_g band between 1 and 2.5 eV. For these bands, not only the band dispersion, but also the bandwidth varies quite a lot. Interestingly, other bands remain more or less

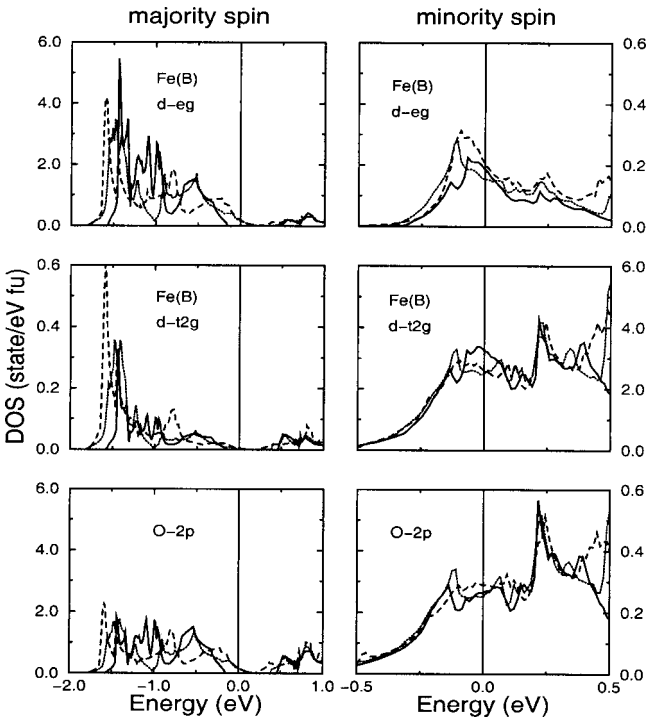

FIG. 5. Orbital-decomposed densities of states near the Fermi level for strained Fe_3O_4. The dotted, solid, and dashed curves indicate the density of states per formula unit under lateral strains of -3.1%, 0.0%, and 3.6%, respectively.

unchanged. For the majority spin, the width of the Fe(B) $3d$-e_g band becomes larger under strain, especially near the Γ point. At both strains, the band top at the Γ point already exceeds the Fermi level and almost touches the lower edge of the upper A-site $3d$-e_g band. For the minority spin, all band edges, as shown in Fig. 4, already overlap and form a large conduction band for both the strains. Figure 5 is a close comparison of the DOS near the Fermi level under strain. Note that the horizontal scales are different for the majority and minority spins, and the vertical scales of the majority Fe(B) d-t_{2g} and minority Fe(B) d-e_g and O $2p$ panels are 10 times smaller than the other panels. For the minority spin, the DOS of the conducting Fe(B) $3d$-t_{2g} band at the Fermi level is slightly reduced under either strain, whereas the DOS at the Fermi level for both the Fe(B) $3d$-e_g and O $2p$ bands are slightly reduced for the negative strain and increased for the positive strain. It can also be seen that the conducting Fe(B) $3d$ band hybridizes with O $2p$ orbitals by about 10% at the Fermi level. For the majority spin, the insulating band gap is closed by the broadening of the Fe(B) $3d$-e_g and O $2p$ bands under both strains (Fig. 5).

It is obvious from the above discussion that an insulator-metal transition would occur in the majority spin as the strain is increased. This is demonstrated in Fig. 6 where we plot the majority-spin band edges of the lower B-site $3d$ band along with the upper A-site $3d$ band as a function of strain. For high compressive ($\varepsilon < -1.3\%$) and high extensive ($\varepsilon > 2.1\%$) strains, the upper edge of the broadening B-site $3d$ band would go above the Fermi level. As a result, the half-metallic behavior would turn into a normal metal state in

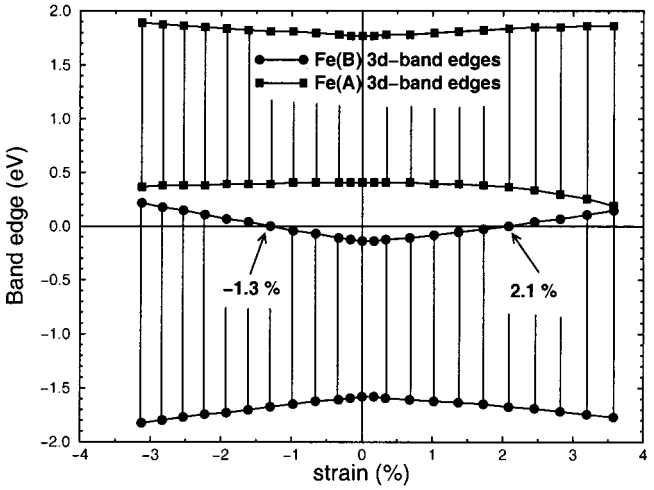

FIG. 6. Majority-spin band edges of Fe_3O_4 near the Fermi level as a function of the lateral strain. The zero energy is the Fermi level. The lines are a guide to the eye only.

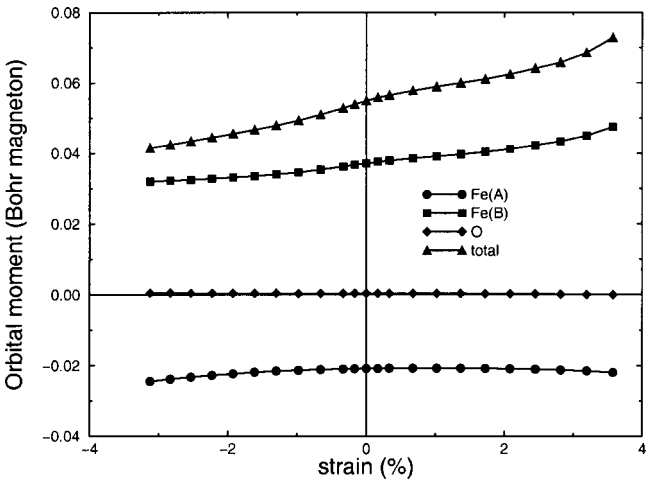

FIG. 7. Total and site-decomposed orbital magnetic moments for [001] magnetization of Fe_3O_4 as a function of the lateral strain. The lines are a guide to the eye only.

these high-strain regimes. Since Fe_3O_4 thin films on a Mn_3O_4 substrate could suffer a strong compressive strain of -3.2%, which is larger than the critical strain of -1.3%, a normal metal behavior would be expected for these films. Another interesting feature is that as the magnitude of either kind of strains increases, there are slightly charge transfer from the oxygen and the *A*-site Fe atoms to the *B*-site Fe atoms. However, there is no abrupt increase in the charge transfer across the critical strains of -1.3% and 2.1%.

Let us now turn to the effects of the strains on magnetism in magnetite. In the small strain region ($-1.3\% < \varepsilon < 2.1\%$), the total spin moment is a constant of $4\mu_B$/f.u. However, in this region the size of the spin moments for both the *A*- and *B*-site Fe atoms is reduced slightly as the strain increases. Accompanied by the transformation from a half-metallic to a normal metal state under high strains, Fe_3O_4 shows a small reduction in the total magnetic moment. The total and site-decomposed orbital magnetic moments for the [001] magnetization as a function of strain are displayed in Fig. 7. Remarkably, the total orbital moment increases substantially as the strain goes from the negative to positive values. Clearly, this is due to the monotonical increase of the Fe(*B*) orbital moments. These changes of the orbital moments under the strains are closely related to that of the magnetocrystalline anisotropy energies, as will be discussed in the next subsection.

C. Anisotropy constants versus strain

The calculated cubic anisotropy constant K_1 (solid circle) of the magnetite as a function of strain is shown in Fig. 8(a). The magnitude of K_1 decreases from -4.7×10^5 erg/cm^3 for a strain of -3.1% to -1.3×10^5 erg/cm^3 for a strain of 2.8%. The negative values of K_1 imply that for all the considered strains the [110] orientation rather than the [100] orientation within the layers is the preferred magnetization direction for an Fe_3O_4 film. Under symmetry considerations, the negative value of K_1 in the cubic limit also indicates that [111], [110], and [001] are, respectively, the easy, intermediate, and hard directions of magnetization of the fcc Fe_3O_4. This is in agreement with the experiments[22] that the four equivalent [111] directions are the magnetic easy axes of the bulk Fe_3O_4 at room temperature. The vanishing K_1 in the high-positive-strain limit indicates that in the transformation from the cubic to the uniaxial symmetry, it is somehow suppressed by the supposedly unrelated uniaxial anisotropy due to the uniaxial strains. This suppression of K_1 has been recently observed in epitaxial fcc Co(110) films on Cu(110).[50]

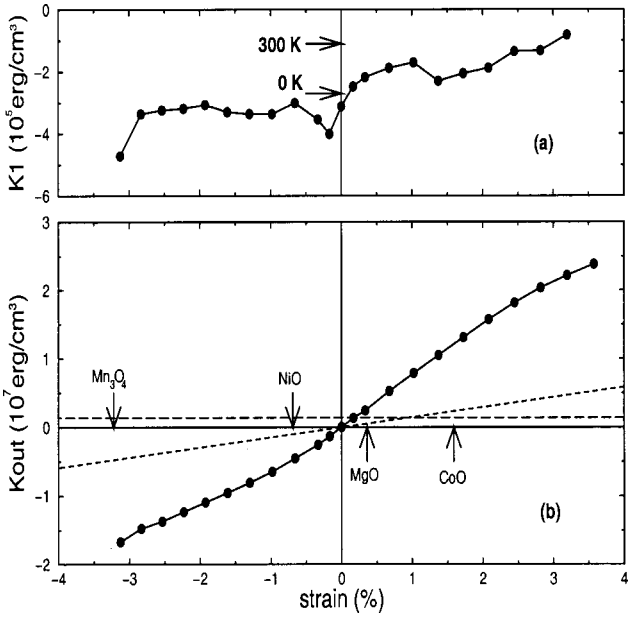

FIG. 8. The fourth-order anisotropy constant K_1 (a) and the out-of-plane anisotropy constant K_{out} (b) as a function of the lateral strain in the (001) plane of Fe_3O_4. The lines are a guide to the eye only. The arrows in (a) indicate the experimental K_1 value at 300 K and 0 K (see text). The arrows in (b) indicate the possible strain values if an Fe_3O_4 film is grown on Mn_3O_4, NiO, MgO, and CoO substrates, respectively.

In zero strain, the calculated K_1 equals -3.1×10^5 erg/cm^3 (-14 μeV/f.u.), which is of the same sign and of the same order of magnitude as the experimental value of -1.1×10^5 erg/cm^3 at 300 K for the high-temperature phase.[2] The experimental K_1 for the unstrained Fe_3O_4 at 300 K as well as the K_1 at 0 K estimated by extrapolation as discussed below, are indicated in Fig. 8(a). The measured dependence of the K_1 on temperature T (Refs. 34 and 35) shows that K_1 is positive below the Verwey transition temperature ($\sim$120 K). As temperature increases, K_1 decreases into negative values rapidly until it reaches the minimum value at about 230 K. Meanwhile, in the high-temperature regime ($T>270$ K), K_1 increases about linearly with temperature. Since the bending of K_1 in the low-temperature region is caused by the Verwey transition, one could extrapolate K_1 linearly from the high-temperature ($T\geqslant300$ K) region towards zero temperature in order to evaluate the K_1 at 0 K for the high-temperature cubic phase of Fe_3O_4. The value of K_1 at 0 K thus estimated is about -2.7×10^5 erg/cm^3,[34,35] being in good agreement with the calculated K_1. The anisotropy constant K_1 is a very small quantity and is the most difficult quantity to calculate. The good agreement between the experimental K_1 and the calculated cubic K_1 could be fortuitous. We have also calculated the anisotropy energies with 18 empty spheres included (4 in positions 16*c* of space group $Fd3m$, 2 in the positions 8*b*, and 12 in the positions 48*f* with $x=1/4$) for the cubic and some strained cases. Although including empty spheres in the calculations enhances the magnitudes of K_1, they are still of the same sign and of the same order of magnitude as the experimental K_1. Also, the trend with respect to strains remains unchanged.

The calculated out-of-plane anisotropy constant $K_{\rm out}$ (solid circle) as a function of strain is shown in Fig. 8(b). The corresponding strains for Mn_3O_4, NiO, MgO, and CoO substrates are also indicated in the figure. The $K_{\rm out}$ increases monotonically from negative to positive strains with the magnitude in the extensive strain regime being slightly larger than that in the compressive strain regime. The $K_{\rm out}$ curve shows more or less piecewise linearities in the strain intervals: $<-0.5\%$, -0.5%–2%, and $>2\%$. Neglecting the shape anisotropy, the negative values of $K_{\rm out}$ for the negative strains indicate that a Fe_3O_4 thin film on a substrate with a smaller lattice constant such as Mn_3O_4 and NiO would prefer an in-plane magnetization. On the other hand, for an Fe_3O_4 film on a substrate of larger lattice constant such as MgO and CoO, the positive $K_{\rm out}$ implies that the out-of-plane magnetization orientation would be preferred. The shape anisotropy energy for a magnetite film is about 1.4×10^6 erg/cm^3 (Ref. 37) and always prefers an in-plane magnetization. The shape anisotropy energy should be almost a constant since the magnetization is nearly independent of the film strain and is plotted as the horizontal dashed line in Fig. 8(b). This means that the strained magnetite film, having a $K_{\rm out}$ above this dashed line, would prefer the perpendicular magnetization. Figure 8(b) suggests that an Fe_3O_4 film under an extensive strain greater than 0.2% would exhibit the perpendicular magnetization. This is in agreement with the recent observation of an out-of-plane moment distribution in Fe_3O_4 films on MgO (0.36%) substrates by conversion electron Mössbauer spectroscopy[22,37] (CEMS) and in Fe_3O_4/MgO superlattices by ferromagnetic resonance (FMR).[51] In particular, the preliminary FMR measurements[51] suggest that the $K_{\rm out}$ of Fe_3O_4 ($\leqslant$60 Å)/MgO superlattices is in the same order of magnitude as the theoretical value. The perpendicular magnetization has also been found in Fe_3O_4 films on CoO (1.59%) substrates.[52]

The strain-induced magnetocrystalline anisotropy in a magnetic film is often estimated by the corresponding bulk magnetostriction coefficient (e.g., λ_{100}) and elastic constants (e.g., C_{11} and C_{12}). Also shown in Fig. 8(b) is the anisotropy constant $K'_{\rm out}$ as a function of strain ε (dotted line) estimated using these bulk constants at room temperature[2] via

$$K'_{\rm out}=-\frac{9}{2}(C_{11}-C_{12})\lambda_{100}\varepsilon. \tag{7}$$

Figure 8(b) shows that the estimated $K'_{\rm out}$ is in qualitative agreement with the results of the *ab initio* calculations (solid circles). However, it is about 4 times smaller in magnitude than the theoretical $K_{\rm out}$ [Fig. 8(b)]. The discrepancy is partly due to the use of room-temperature λ_{100} and C_{11} and C_{12}, and partly, we believe, due to the fact that the strain-induced anisotropy might not be accurately derived from the bulk magnetostriction constant. In particular, the latter reason could well be the major origin of the *anomalous* magnetic behavior observed by CEMS in Fe_3O_4 films on MgO substrates.[22,37] Figure 8(b) indicates that the estimated $K'_{\rm out}$ plus the shape anisotropy would predict an in-plane magnetization for these films, in contradiction to the CEMS results. On the other hand, the calculated $K_{\rm out}$ plus the shape anisotropy would suggest the perpendicular magnetization for Fe_3O_4 films on MgO substrates, in agreement with the experiments.[22,37]

To gain insight into the source of the $K_{\rm out}$, we plot in Fig. 9(a) the site-decomposed anisotropy energies between [100] and [001] directions of magnetization as a function of strain. The partial contributions to the anisotropy energy were obtained as the differences in the site-decomposed eigenvalue sums between [100] and [001] magnetization directions according to the force theorem. Interestingly, Fig. 9(a) shows that the contributions from an Fe(A) atom and an Fe(B) atom have about the same size but are opposite in sign, despite the rather different electronic structures near the Fermi level for these two kinds of iron atoms (Figs. 2 and 3). As can be expected, the contribution from an oxygen atom is small [Fig. 9(a)]. Since the *B*-site iron atoms are twice as many as the *A*-site iron atoms, the sign of the $K_{\rm out}$ is determined by the anisotropy of the Fe(B) atoms and the value is approximately equal to half of the sum of the Fe(B) anisotropy energies. It has been demonstrated that because the orbital magnetic moment and the magnetocrystalline anisotropy energy are both due to the spin-orbit coupling, they are intimately connected.[53] In particular, the easy axis is along the direction in which the orbital moment has the largest value. To see possible correlations between the anisotropy energy and orbital moment anisotropy in magnetite, we dis-

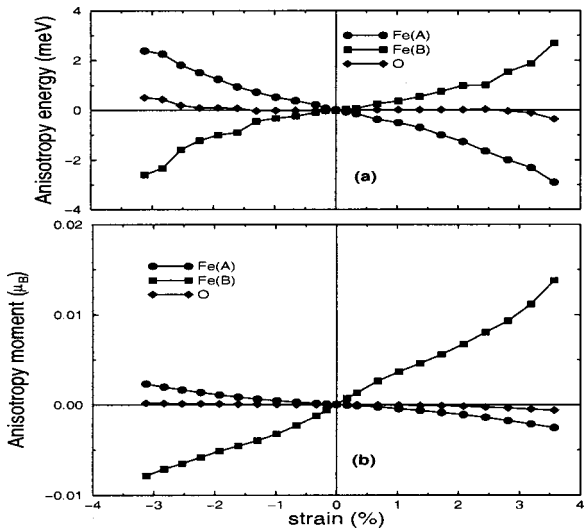

FIG. 9. Site-decomposed anisotropy energies between the [100] and [001] directions of magnetization for Fe_3O_4 as a function of the lateral strain (a) and site-decomposed orbital moment anisotropy between [001] and [100] directions as a function of the lateral strain (b).

play the site-decomposed orbital moment anisotropies between the [001] and [100] directions of magnetization as a function of strain in Fig. 9(b). It is clear that all the site-decomposed orbital moment anisotropies agree with the site-decomposed anisotropy energies in sign (see Fig. 9): i.e., in the direction in which the orbital moment is larger, the energy is lower. The orbital moment anisotropy of the oxygen atoms (diamonds) is again negligibly small.

IV. CONCLUSIONS

We have calculated the electronic structure and magnetocrystalline anisotropy energies of the magnetite (Fe_3O_4) under both compressive and extensive uniaxial strains along [001] direction from first principles by using the LMTO method. The calculated band structure of the unstrained fcc magnetite is compatible with the published *ab initio* calculations.[4,5,25,26] The calculated cubic anisotropy constant K_1 is also in fair agreement with experiments.[34,35] It is found that the uniaxial strains have significant effects on both the electronic structure and magnetocrystalline anisotropy of magnetite. In particular, as the uniaxial strain is applied, the insulating band gap of the majority spin is reduced due to the broadening of the *B*-site Fe $3d$ band. The half-metallic behavior of the cubic magnetite eventually turns into normal metal behavior in the high-strain regimes ($\varepsilon > 2.1\%$, $\varepsilon < -1.3\%$), accompanied by a small reduction of the total magnetic moment from an integer value of $4\mu_B$/f.u.

The increasing extensive lateral strain would not only induce a perpendicular magnetocrystalline anisotropy (the positive K_{out}), but also somehow suppress the seemingly unrelated cubic anisotropy K_1. The compressive lateral strains would cause an in-plane magnetocrystalline anisotropy. The calculated anisotropy constant K_{out} depends monotonically on the lateral strain. The theoretical results for the extensive lateral strains are in overall good agreement with recent magnetic anisotropy measurements on Fe_3O_4 films on MgO and CoO substrates.[22,37,51,52] Interestingly, the contributions from an Fe(A) atom and an Fe(B) atom to the uniaxial anisotropy have about the same size, but are opposite in sign, while the contribution from an oxygen atom is small. However, the sign of the uniaxial anisotropy is determined by the anisotropy of the Fe(B) atoms, since the *B*-site iron atoms are twice as many as the *A*-site iron atoms. It is also found that the sign of each site-decomposed anisotropy energy follows the sign of the corresponding site-decomposed orbital moment anisotropy. This suggests that one could use experiments such as element-specific x-ray magnetic circular dichroism, which can determine the orbital moment anisotropy,[54] to determine the magnetocrystalline anisotropy of magnetite films.

ACKNOWLEDGMENTS

This work was supported by the National Science Council of the Republic of China (Grant Nos. NSC89-2119-M-007-011, NSC89-2112-M002-0025, -0089). The authors thank Dr. J. G. Lin for stimulating discussions and also for making her experimental results available prior to publication.

*Electronic address: jeng@phys.nthu.edu.tw
†Electronic address: gyguo@phys.ntu.edu.tw

[1] E. J. W. Verwey and E. L. Heilmann, J. Chem. Phys. **15**, 174 (1947); E. J. W. Verwey, P. W. Haayman, and F. C. Romeijn, *ibid.* **15**, 181 (1947).
[2] *Magnetic and Other Properties of Oxides and Related Compounds*, edited by K. H. Hellwege, Landolt-Börnstein, New Series, Group III, Vol. 4, Pt. b (Springer-Verlag, New York, 1970).
[3] Z. Kąkol and J. M. Honig, Phys. Rev. B **40**, 9090 (1989).
[4] A. Yanase and K. Siratori, J. Phys. Soc. Jpn. **53**, 312 (1984).
[5] M. Pénicaud, B. Siberchicot, C. B. Sommers, and J. Kübler, J. Magn. Magn. Mater. **103**, 212 (1992).
[6] J. Yoshida and S. Iida, J. Phys. Soc. Jpn. **42**, 230 (1977); S. Iida, Philos. Mag. B **42**, 349 (1980).
[7] M. Iizumi, T. F. Koetzle, G. Shirane, S. Chikazumi, M. Matsui, and S. Todo, Acta Crystallogr., Sect. B: Struct. Crystallogr. Cryst. Chem. **38**, 2121 (1982).
[8] N. F. Mott, Adv. Phys. **16**, 49 (1967).
[9] J. M. Zuo, J. C. H. Spence, and W. Petuskey, Phys. Rev. B **42**, 8451 (1990).
[10] V. I. Anisimov, I. S. Elfimov, N. Hamada, and K. Terakura, Phys. Rev. B **54**, 4387 (1996).
[11] S. B. Ogale, K. Ghosh, R. P. Sharma, R. L. Greene, R. Ramesh, and T. Venkatesan, Phys. Rev. B **57**, 7823 (1998).
[12] J. J. Krebs, D. M. Lind, E. Lochner, K. A. Shaw, W. Portwine, and S. D. Berry, J. Appl. Phys. **75**, 6688 (1994).
[13] R. Jansen, H. van Kempen, and R. M. Wolf, J. Vac. Sci. Technol. B **14**, 1173 (1996).
[14] J. F. Anderson, M. Kuhn, U. Diebold, K. Shaw, P. Stoyanov, and D. Lind, Phys. Rev. B **56**, 9902 (1997).

[15] P. Stoyanov, A. Gottschalk, and D. M. Lind, J. Appl. Phys. **81**, 5010 (1997).
[16] K. Siratori, Y. Ishii, Y. Morii, and S. Funahashi, J. Phys. Soc. Jpn. **67**, 2818 (1998).
[17] Y. Q. Cai, M. Ritter, W. Weiss, and A. M. Bradshaw, Phys. Rev. B **58**, 5043 (1998).
[18] F. C. Voogt, T. T. M. Palstra, L. Niesen, O. C. Rogojanu, M. A. James, and T. Hibma, Phys. Rev. B **57**, R8107 (1998).
[19] C. A. Kleint, M. K. Krause, R. Höhne, T. Walter, H. C. Semmelhack, M. Lorenz, and P. Esquinazi, J. Appl. Phys. **84**, 5097 (1998).
[20] F. Schedin, L. Hewitt, P. Morrall, V. N. Petrov, G. Thornton, S. Case, M. F. Thomas, and V. M. Uzdin, Phys. Rev. B **58**, R11 861 (1998).
[21] S. K. Shaikhutdinov, M. Ritter, X. G. Wang, H. Over, and W. Weiss, Phys. Rev. B **60**, 11 062 (1999).
[22] F. C. Voogt, T. Fujii, P. J. M. Smulders, L. Niesen, M. A. James, and T. Hibma, Phys. Rev. B **60**, 11 193 (1999).
[23] M. L. Rudee, D. J. Smith, and D. T. Margulies, Phys. Rev. B **59**, R11 633 (1999).
[24] G. Chern, L. Horng, T. Y. Hou, and M. Z. Lin, Appl. Phys. Lett. **76**, 598 (2000).
[25] R. A. de Groot and K. H. J. Buschow, J. Magn. Magn. Mater. **54–57**, 1377 (1986).
[26] Z. Zhang and S. Satpathy, Phys. Rev. B **44**, 13 319 (1991).
[27] S. G. Bishop and P. C. Kemeny, Solid State Commun. **15**, 1877 (1974).
[28] K. Siratori, S. Suga, M. Taniguchi, K. Soda, S. Kimura, and A. Yanase, J. Phys. Soc. Jpn. **55**, 690 (1986).
[29] S. F. Alvarado, W. Eib, F. Meier, D. T. Pierce, K. Sattler, H. C. Siegmann, and J. P. Remeika, Phys. Rev. Lett. **34**, 319 (1975).
[30] V. C. Rakhecha and N. S. S. Murthy, J. Phys. C **11**, 4389 (1978).
[31] J. Garcia, G. Subias, M. G. Proietti, H. Renevier, Y. Joly, J. L. Hodeau, J. Blasco, M. C. Sanchez, and J. F. Berar, Phys. Rev. Lett. **85**, 578 (2000).
[32] L. R. Bickford, Jr., Phys. Rev. **76**, 137 (1949); **78**, 449 (1950); L. R. Bickford, J. M. Brownlow, and R. F. Penoyer, Proc. Inst. Electr. Eng. **104B**, Suppl. No. 5, 238 (1957).
[33] W. Palmer, Phys. Rev. **131**, 1057 (1963).
[34] K. Abe, Y. Miyamoto, and S. Chikazumi, J. Phys. Soc. Jpn. **41**, 1894 (1976).
[35] R. Aragón, Phys. Rev. B **46**, 5334 (1992).
[36] Z. Kąkol, J. Sabol, J. Stickler, A. Kozłowski, and J. M. Honig, Phys. Rev. B **49**, 12 767 (1994).
[37] D. T. Margulies, F. T. Parker, F. E. Spada, R. S. Goldman, J. Li, R. Sinclair, and A. E. Berkowitz, Phys. Rev. B **53**, 9175 (1996).
[38] G. H. D. Daalderop, P. J. Kelly, and M. F. H. Schuurmans, Phys. Rev. B **41**, 11 919 (1990); **42**, 7270 (1990).
[39] G. Y. Guo, W. M. Temmerman, and H. Ebert, J. Phys.: Condens. Matter **3**, 8205 (1991).
[40] A. B. Shick, D. L. Novikov, and A. J. Freeman, Phys. Rev. B **56**, R14 259 (1997).
[41] G. Y. Guo, D. J. Roberts, and G. A. Gehring, Phys. Rev. B **59**, 14 466 (1999).
[42] O. K. Andersen, Phys. Rev. B **12**, 3060 (1975).
[43] S. H. Vosko, L. Wilk, and M. Nusair, Can. J. Phys. **58**, 1200 (1980).
[44] H. C. Hamilton, Phys. Rev. **110**, 1050 (1958).
[45] O. Jepson and O. K. Andersen, Solid State Commun. **9**, 1763 (1971); W. M. Temmerman, P. A. Sterne, G. Y. Guo, and Z. Szotek, Mol. Simul. **4**, 153 (1989).
[46] R. H. Victora and J. M. MacLaren, Phys. Rev. B **47**, 11 583 (1993).
[47] M. Kim, L. Zhong, and A. J. Freeman, Phys. Rev. B **57**, 5271 (1998).
[48] G. Y. Guo, W. M. Temmerman, and H. Ebert, Physica B **172**, 61 (1991).
[49] X. Wang, D. S. Wang, R. Wu, and A. J. Freeman, J. Magn. Magn. Mater. **159**, 337 (1996).
[50] B. Hillebrands, J. Fassbender, R. Jungblut, G. Güntherodt, D. J. Roberts, and G. A. Gehring, Phys. Rev. B **53**, R10 548 (1996).
[51] J. G. Lin *et al.* (unpublished).
[52] P. J. H. Bloemen, P. A. A. Van der Heijden, R. M. Wolf, J. aan de Stegge, J. T. Kohlhepp, A. Reinders, R. M. Jungblut, P. J. van der Zaag, and W. J. M. de Jonge, in *Epitaxial Oxide Thin Films II*, edited by D. K. Fork, G. S. Speck, T. Shiusaki, and R. M. Wolf, Mater. Res. Soc. Symp. Proc. No. 401 (Materials Research Society, Pittsburgh, 1996), p. 485.
[53] P. Bruno, Phys. Rev. B **39**, 865 (1989).
[54] H. A. Dürr, G. Y. Guo, G. van der Laan, J. Lee, G. Lauhoff, and J. A. C. Bland, Science **277**, 213 (1997).